AUTOMATIC ESTIMATION OF REGION OF INTEREST AREA IN DERMATOLOGICAL IMAGES USING DEEP LEARNING AND PIXEL-BASED METHODS: A CASE STUDY ON WOUND AREA ASSESSMENT

R-D. Berndt [1], C. Takenga [1], P. Preik [1], T. Siripurapu [1], T. Fuchsluger [2], C. Lutter [3], A. Arnold [4], S. Lutze [4]

[1] INFOKOM – Informations- und Kommunikationsgesellschaft mbH, Nonnenhofer Straße 4a, 17033 Neubrandenburg, Germany
[2] Clinic and Polyclinic of Ophthamology, Medical University of Rostock, Doberaner Straße 140, 18057 Rostock, Germany
[3] Clinic and Polyclinic for Orthopedy, Medical University of Rostock, Doberaner Straße 142, 18057 Rostock, Germany
[4] Clinic and Polyclinic for Skin Diseases, Medical University of Greifswald, Ferdinand-Sauerbruch-Str. 1, 17475 Greifswald, Germany

ABSTRACT

Accurate wound area estimation is essential for effective dermatological assessment and treatment monitoring. However, manual measurement is time-consuming and error-prone, highlighting the need for automated, reliable methods. This paper aims to develop and evaluate two complementary techniques for estimating the Region of Interest (ROI) in dermatological images: a novel deep learning approach using the Segment Anything Model (SAM) and a simple pixel-based thresholding method. SAM segments both the wound and a reference object automatically or through prompt-based queries, without requiring additional supervised classification. The pixel-based method offers a lightweight alternative for resource-limited settings. Both techniques generate binary masks and calculate real-world areas using a pixel-to-centimeter scale. Evaluation on 40 images shows that SAM outperforms the pixel-based method, achieving an average relative error of 4.63% versus 9.5% and ≤5% error in 62.5% of cases compared to 27.5%. The proposed methods are not limited to wound area estimation but can be extended to inflammation area detection in rheumatoid arthritis and ophthalmology, providing a scalable framework for ROI estimation in medical imaging.

KEYWORDS

Region of Interest (ROI) Detection, Wound Area Estimation, Pixel-Based Measurement, Segment Anything Model (SAM), Artificial Intelligence in Dermatology

1. INTRODUCTION

Precise wound area estimation is critical for effective clinical assessment in dermatology, as it directly informs diagnosis, treatment planning, and the monitoring of healing progress. Accurate measurement enables clinicians to track changes over time, evaluate treatment effectiveness, and adapt interventions, particularly for chronic wounds, burns, and diabetic ulcers.

Traditional wound area estimation methods often rely on manual techniques, such as ruler-based measurements or tracing on transparent film. While these can be useful, they are prone to human error, time-consuming, and limited in precision, especially when dealing with irregular wound shapes or large patient volumes. Manual methods are also subject to inter-observer variability, reducing consistency in assessments.

To overcome these limitations, image-based approaches have gained traction. Pixel-based techniques leverage digital image analysis to quantify wound areas using intensity thresholds and geometrical scaling, offering a more reproducible and objective alternative. In parallel, advances in deep learning, particularly models like the Segment Anything Model (SAM), allow for automated detection and segmentation of both reference objects and wound regions directly from images. These methods provide improved accuracy and robustness across varied imaging conditions and patient presentations.

Together, these approaches offer flexible solutions that can streamline clinical workflows, reduce subjectivity, and improve the reliability of dermatological assessments.

The objective of this study is to present two methods for the automatic estimation of wound area in dermatological images: one based on deep learning, and the other on pixel-based thresholding techniques. The deep learning approach employs the Segment Anything Model (SAM) to detect and segment both the reference object (used for real-world scaling) and the wound area. In contrast, the pixel-based method uses intensity-based thresholding to isolate regions of interest in simpler imaging conditions.

Rather than comparing the two approaches, the study aims to demonstrate their complementary value in different clinical and technical contexts. The goal is to provide practical, accurate, and reproducible tools for wound area assessment, tools that can be adapted depending on resource availability, image quality, and application requirements.

Additionally, the methods introduced in this study are designed to be applicable beyond wound care, for example, in rheumatoid arthritis, where detecting and quantifying inflamed regions in hand joints is essential for clinical evaluation. By enabling automated ROI segmentation and measurement, this work contributes to more objective, scalable, and efficient diagnostic workflows in dermatological imaging. Ultimately, it aims to improve patient care through enhanced diagnostic accuracy, streamlined clinical processes, and reduced reliance on manual measurements, thereby minimizing the risk of human error.

2. RELATED WORKS

Wound area estimation is a critical aspect of dermatological and clinical care, and numerous techniques have been proposed to improve accuracy, efficiency, and objectivity. Traditional manual measurement methods, such as ruler-based and planimetry techniques, though still commonly used in clinical practice, are limited by user subjectivity and inter-observer variability [1], [2]. While these methods offer simplicity, they are not well suited for complex wound shapes or large-scale clinical deployment.

To overcome these limitations, pixel-based and image processing methods have gained prominence. Techniques using reference objects with known dimensions enable wound area estimation based on the pixel ratio, enhancing reproducibility and consistency [3]. However, such approaches remain sensitive to lighting, image resolution, and wound boundary contrast.

With advances in artificial intelligence (AI), deep learning-based techniques have revolutionized medical image analysis, offering robust capabilities for automatic detection and segmentation of regions of interest (ROIs). Convolutional neural networks (CNNs) have shown remarkable accuracy in identifying wound boundaries and measuring wound size [4], [5]. Several recent studies have explored the development of deep learning architectures for wound analysis, including segmentation models, attention mechanisms, and hybrid systems. For instance, Carrión et al. demonstrated the use of deep learning algorithms to automate wound detection and monitor healing [6], [7]. Similarly, Chairat et al. proposed a detect-and-segment architecture for accurate ROI identification [8], while Chang et al. developed superpixel-based CNN models to enhance segmentation accuracy in pressure ulcers [9]. Foltynski and Ladyzynski further evaluated the performance of AI-based digital wound area measurements [10]. Chino et al. explored the segmentation of skin ulcers using deep convolutional networks, emphasizing the importance of architectural design in clinical accuracy [11].

The use of smartphone-based and 3D imaging methods has also been explored for mobile and low-resource applications. Liu et al. proposed a smartphone image-based 3D transformation approach for wound area measurement [12], while Ferreira et al. validated mobile device capabilities in this context [13]. Other innovations include integration with LiDAR technology [14] and evaluation of AI-based measurement accuracy compared to clinical standards [15].

Recent studies have applied the Segment Anything Model (SAM) to improve generalizability across different wound types and imaging scenarios. SAM's zero-shot capabilities allow it to segment without prior task-specific training, making it highly versatile [16]. Additionally, public platforms such as Labellerr have implemented SAM and other advanced models to improve annotation quality in wound datasets [17].

Thermal imaging and machine learning are also gaining traction for broader clinical ROI detection beyond dermatology. Morales-Ivorra et al. and Snekhalatha et al. demonstrated that thermographic data, analyzed through machine learning, can be used to assess inflammation in rheumatoid arthritis [18], [19]. Wilson et al. presented a comprehensive review of recent thermal imaging applications supported by machine learning, highlighting innovations relevant to diagnostics in inflammatory and oncologic conditions [20]. Similarly, studies have applied thermal imaging with CNNs for breast cancer detection [21], [22], pneumonia monitoring [23], and eye inflammation evaluation [24]. Qu et al. showed that low-cost thermal imaging combined with machine learning enables non-invasive diagnosis in pulmonary conditions [23]. A survey by Wang et al. outlines the growing applications of AI in rheumatoid arthritis diagnostics [25], and Morales-Ivorra et al. later validated machine learning-based thermographic indices through a longitudinal study [26].

Emerging platforms such as Deepwound [27], mobile applications for localization [28], and hybrid segmentation approaches [29] further demonstrate the variety and accessibility of modern wound analysis tools. Nejati et al. explored fine-grained wound tissue classification with deep networks [30], contributing to tissue-level analytics. The integration of depth and ambient intelligence systems for patient care, including dementia and ophthalmic applications, reflects the expanding potential of intelligent imaging across medical disciplines [31].

Collectively, these advances demonstrate a clear trend toward automation, reproducibility, and adaptability in wound and ROI analysis. This study builds on this foundation by introducing two complementary approaches: a pixel-based method for lightweight applications and a SAM-based deep learning framework for scalable and accurate segmentation, bridging gaps in resource accessibility and clinical generalization. While these approaches show great promise, challenges remain. Many deep learning solutions depend heavily on large annotated datasets and complex

model training, which limit their scalability and deployment in clinical settings, especially in low-resource environments. Furthermore, most models are trained on narrow datasets, affecting their ability to generalize across wound types, skin tones, and imaging conditions.

3. METHODOLOGY

3.1. Pixel-Based Method for Automated ROI Estimation

3.1.1. Principle of Wound Area Size calculation using pixels

The principle of area calculation using pixels is based on the ratio of the number of pixels representing two surfaces: the object (whose area we want to calculate) and a reference surface with a known area. This concept is commonly used in digital image processing and geometric calculations in 2D images.

Defining areas as pixel counts: In a digital image, each surface is represented by a number of pixels. The pixel count can be obtained through an image processing technique, such as segmentation or thresholding.

- The number of pixels representing the object (the area to be determined) is denoted as N_{obj}
- The number of pixels representing the reference area is denoted as N_{ref}

Known reference area: The actual area of the reference figure is known and is denoted as A_{ref}.

This serves as a scale for calculating the area of the object A_{obj}

Ratio of pixel counts: The ratio of the pixel count of the object to the pixel count of the reference area can be used to determine the ratio of the actual areas. The ratio of the areas is proportional to the ratio of the pixel counts since the pixel size is the same for both areas.

$$\frac{A_{obj}}{A_{ref}} = \frac{N_{obj}}{N_{ref}} \tag{1}$$

Calculating the object's area: To determine the object's area A_{obj}, the formula is rearranged:

$$A_{obj} = A_{ref} \cdot \frac{N_{obj}}{N_{ref}} \tag{2}$$

Here, the actual area of the reference figure A_{ref} is multiplied by the ratio of pixel counts to calculate the object's area.

It is assumed that:

- Both areas (reference and object) must lie in the same plane of the image, and the pixel sizes must be identical.
- The image resolution and the pixel-to-area ratio must remain constant for an accurate calculation.

This method of determining area is particularly useful when direct physical measurement of the object's area is not feasible, but the pixel count can be easily extracted from image data.

3.1.2. Strategy for Enhancing Accuracy in ROI Area Size Estimation

Discussion of shape-based errors in pixel estimation:

- Square vs. circle pixel approximations and their effects.

In the context of area calculation using pixels, the accuracy of measurements depends on the shape being represented. For a square, the pixel count precisely matches the square's area, resulting in no error (Fig. 1). However, real errors may arise due to challenges in edge detection. For a circle, the situation is different. Due to the rounded shape, some pixels along the edges of the circle may be only partially or excessively counted, leading to measurement errors. This error occurs because a circle is being represented by square pixels, creating an approximation problem. When attempting to depict a circular shape using square pixels, the mismatch between the shape and the pixel grid introduces a degree of inaccuracy in the area estimation (Fig.1).

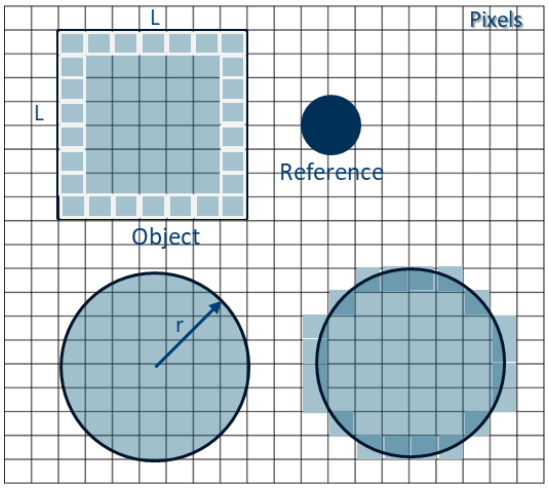

Fig.1: Pixel-Based Representation of Objects and Reference Markers for Area Estimation, Error in pixel numbers due to shape

Error propagation due to reference area inaccuracies.

Case 1. Error in the reference area measurement ε_{ref} and its impact on the object area:

When an error ε_{ref} is present in the reference area A_{ref}, the erroneous reference area becomes $A_{ref} + \varepsilon_{ref}$. This alters the calculated object area A'_{obj} to:

$$A'_{obj} = \left(A_{ref} + \varepsilon_{ref}\right) \cdot \frac{N_{obj}}{N_{ref}} \tag{3}$$

This shows that any error in the reference area directly propagates to the calculated object area in proportion to the ratio of the pixel counts.

The difference between the actual object area A_{obj} and the erroneously calculated object area represents the error in the object area, denoted as ε_{obj}. By substituting the corresponding expressions, we get:

$$\varepsilon_{obj} = \left(A'_{obj} - A_{obj}\right) \tag{4}$$
$$\varepsilon_{obj} = \left(\left(A_{ref} + \varepsilon_{ref}\right) \cdot \frac{N_{0bj}}{N_{ref}}\right) - \left(A_{ref} \cdot \frac{N_{obj}}{N_{ref}}\right)$$

$$\varepsilon_{obj} = \varepsilon_{ref} \cdot \frac{N_{obj}}{N_{ref}} \tag{5}$$

This means that the error in the object area ε_{obj} is proportional to the error ε_{ref} in the reference area and the ratio of pixel counts. A larger error in the reference area will result in a correspondingly larger error in the calculated object area.

The larger the object is in comparison to the reference area, the more significantly a small error in the reference area will affect the calculated object area. Therefore, it is especially important to ensure precise measurements of the reference area, particularly when dealing with large objects relative to the reference, in order to minimize errors.

Case 2. Errors in the pixel counts of object and reference areas:

- *Scenario 1:* Error ε_{obj} only in the pixel counts Covering the Object Area N_{obj}

$$N_{obj,Erroneous} = N_{obj}\left(1 + \varepsilon_{obj}\right) \tag{6}$$

The calculated area of the object then becomes:

$$A_{obj,Erroneous} = A_{ref} \cdot \frac{N_{0bj}(1+\varepsilon_{obj})}{N_{ref}} \tag{7}$$

The relative error in the object area due to the error in the pixel count of the object area is:

$$\Delta A_{obj} = A_{obj,Erroneous} - A_{obj} = A_{obj} . \varepsilon_{obj} \tag{8}$$

The larger this ε_{obj} error in the pixel counts covering the object is, the greater the error in the object area will be.

- *Scenario 2:* Error ε_{ref} only in the pixel counts Covering the Reference Area N_{ref}

$$N_{ref,Erroneous} = N_{ref}\left(1 + \varepsilon_{ref}\right) \tag{9}$$

The calculated area of the object then becomes:

$$A_{obj,Erroneous} = A_{ref} \cdot \frac{N_{0bj}}{N_{ref}(1+\varepsilon_{ref})} \tag{10}$$

The relative error in the object area due to the error in the pixel count of the reference area is:

$$\Delta A_{obj} = A_{obj,Erroneous} - A_{obj} = A_{obj} \cdot \frac{-\varepsilon_{ref}}{1+\varepsilon_{ref}} \quad (11)$$

The larger this ε_{ref} error in the number of pixels covering the reference is, the greater the error in the object area will be.

– *Scenario 3:* Errors ε_{obj} and ε_{ref} in the pixel counts covering both Object Area N_{obj} and Reference Area N_{ref}

$N_{obj,Erroneous} = N_{obj}(1+\varepsilon_{obj})$ and $N_{ref,Erroneous} = N_{ref}(1+\varepsilon_{ref})$
The calculated area of the object then becomes:

$$A_{obj,Erroneous} = A_{ref} \cdot \frac{N_{Obj}(1+\varepsilon_{obj})}{N_{ref}(1+\varepsilon_{ref})} \quad (12)$$

The relative error in the object area due to the error in the pixel count of both areas is:

$$\Delta A_{obj} = A_{obj,Erroneous} - A_{obj} = A_{obj} \cdot \frac{(1+\varepsilon_{obj})}{1+\varepsilon_{ref}} - A_{obj} \quad (13)$$

- *Variant 1:* The error in the number of pixels covering the object area is greater than in the reference area.

  If $\varepsilon_{obj} > \varepsilon_{ref}$, the error in the calculated object area is primarily dominated by the errors in the object pixel count.

- *Variant 2:* The error in the number of pixels covering the reference area is greater than in the object area.

  If $\varepsilon_{ref} > \varepsilon_{obj}$, the error in the reference area has a greater impact on the object area, and the calculated area is typically underestimated.

- *Variant 3:* Equal error in both.

  If $\varepsilon_{obj} = \varepsilon_{ref}$, the errors partially cancel each other out, and the resulting error in the object area will be smaller.

In cases where the object is significantly larger than the reference area, it is imperative that the reference area is measured with the highest possible accuracy to minimize associated errors. Alternatively, selecting a slightly larger reference area may also be beneficial. It is essential that the reference area is not disproportionately small in relation to the object.

If errors arise in the pixel counts covering both the reference and the object areas, it is advisable for these errors to be equal for both surfaces. Achieving this balance is crucial for minimizing the overall error in the calculation of the object area. This implies, when dealing with objects exhibiting round shapes, which may result in larger errors in pixel counts, the reference should

also be designed with a round shape, such as a circle. Conversely, for objects with angular shapes that tend to produce smaller pixel deviations, a square reference area is recommended as the most appropriate choice (Fig.2).

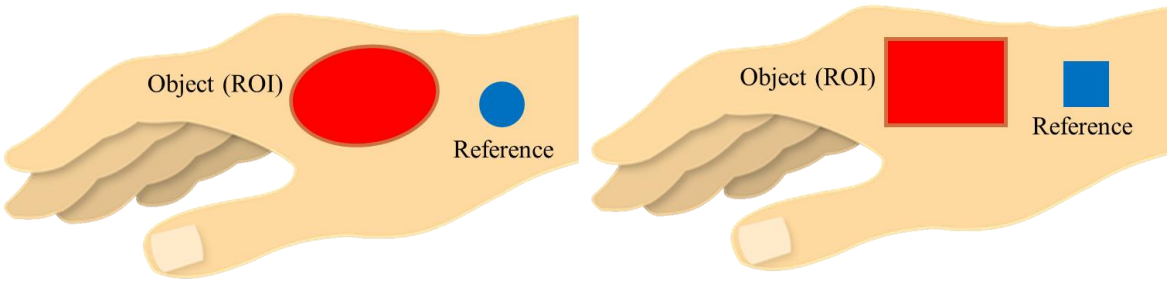

Fig. 2: Selection of Reference Shape According to the Object (ROI) Shape for Accurate Area Estimation

3.2. Deep Learning Approach Using SAM for Automated ROI Estimation

This study employs the Segment Anything Model (SAM), a pretrained and prompt-driven deep learning framework, for automatic segmentation of both the reference object (a blue 1 cm^2 marker) and the wound area in clinical dermatological images. SAM is particularly suited for medical image segmentation tasks due to its flexibility, zero-shot generalization, and prompt-based mask generation.

Model Architecture Overview:

SAM is based on a Vision Transformer (ViT) backbone, which transforms the input image into high-dimensional embeddings. These embeddings are passed to a lightweight mask decoder conditioned on user prompts such as bounding boxes or point annotations. The model generates binary segmentation masks without requiring task-specific fine-tuning.

Workflow and Implementation:

The SAM-based wound assessment pipeline consists of the following stages:

1. Image Input and Preprocessing:
    - Images are loaded and converted to RGB.
    - A 1 cm^2 blue-colored square marker is visually present in the image to enable scale calibration.
2. Model Initialization:
    - The ViT-H variant of SAM is loaded using PyTorch and executed on GPU (or CPU if unavailable).
    - CUDA memory is managed explicitly to avoid allocation errors.
3. Automatic Ruler Segmentation:
    - SAM's SamAutomaticMaskGenerator is used to generate masks for all detected regions in the image.

- Each mask is evaluated to identify a dominantly blue region, presumed to be the reference marker, using HSV color filtering.
- The pixel area of this region is used to derive the real-world pixel-to-centimeter ratio.

4. Wound Segmentation via Manual Bounding Box Prompt:

    - A user-provided bounding box (defined in pixel coordinates) is passed to SamPredictor, which generates a precise mask for the wound area.
    - The mask is post-processed to ensure it fits strictly within the bounding box.

5. Area Calculation:

    - The number of pixels in the wound mask is calculated.
    - Using the previously computed reference scale, the wound area is converted into real-world surface area in cm²:

$$A_{\text{cm}^2} = \frac{A_{px}}{A_{ruler\ px}} \tag{14}$$

    - The final result is presented as a labeled mask overlaid on the original image.

6. Visualization and Output:

    - Segmented areas (wound and reference marker) are highlighted in white on a dimmed background.
    - Annotations are displayed with corresponding area measurements.
    - The final image is visualized using matplotlib and saved for documentation.

Key Advantages:

- Zero-shot segmentation: SAM does not require retraining on medical datasets, making it suitable for clinical environments where labeled data is scarce.
- Prompt flexibility: Supports bounding boxes, points, or fully automatic segmentation.
- Generalization: Effectively segments irregular, variable wound structures without prior domain adaptation.

This structure provides a robust, prompt-based deep learning architecture that supports automated, scalable, and interpretable wound area estimation with minimal manual input.

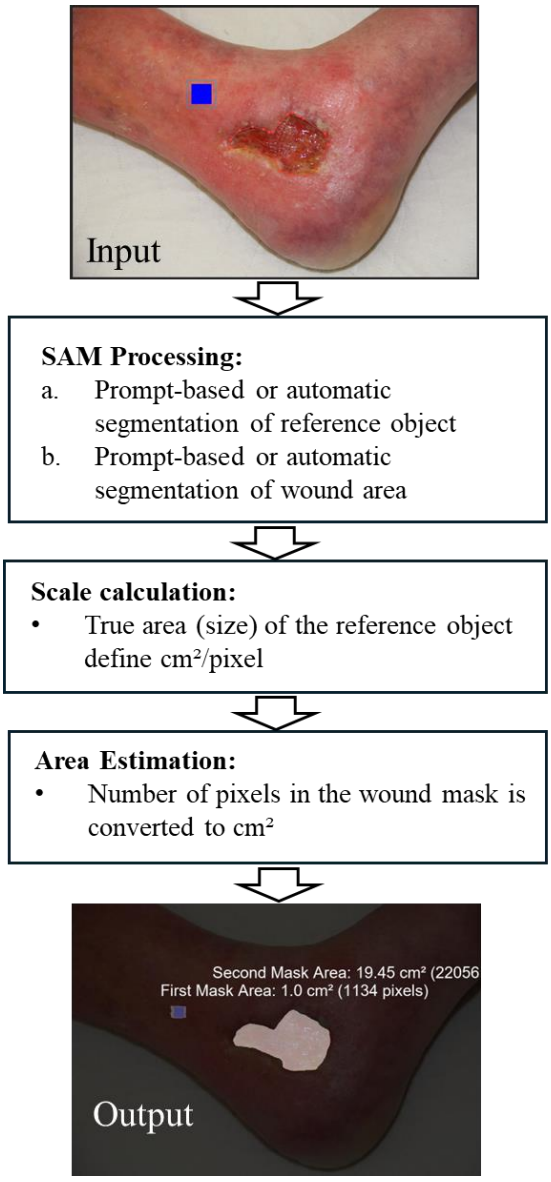

Fig. 3: Workflow Using SAM for Automated ROI Segmentation and Area Estimation

- Input: Dermatological image containing a wound and a reference object (Fig. 3)
- SAM Processing:
  a. Prompt-based or automatic segmentation of reference object
  b. Prompt-based or automatic segmentation of wound area
- Scale Calculation: Real-world dimensions of the reference object define cm²/pixel
- Area Estimation: Number of pixels in the wound mask is converted to cm²
- Output: Real-world wound area estimation

While architectures like U-Net require specific training on labeled wound datasets, SAM avoids this need by leveraging Vision Transformers (ViTs) as its backbone, along with a Mask Decoder that generates segmentation masks based on image embeddings and user prompts (points, boxes, or automatic queries).

This makes SAM highly effective in clinical imaging, where manual annotation is costly, and visual variability is high.

4. EXPERIMENTAL SETUP

4.1. Experimental Design

The experiments were structured in two main phases to evaluate the performance of the proposed ROI area estimation methods using both synthetic and real-world data:

Step 1: Validation with Known Shapes

The first set of experiments was conducted using test figures (printed shapes) of known, pre-measured surface areas. Each image also included a reference marker of 1 cm^2, placed on the same plane as the shape. These artificial setups allowed precise evaluation of the estimation accuracy, as the true areas were known, enabling direct computation of the relative error between the assessed and true areas.

Step 2: Application on Real Wounds

The second set of experiments was performed on images of actual patient wounds, captured in clinical settings. For consistency, a 1 cm × 1 cm blue square marker was affixed near the wound in each image. To minimize perspective distortion, the camera was held parallel to the wound surface during image acquisition. The system estimated not only the surface area of the wound, but also its length and width based on the bounding box of the segmented ROI.

4.2. Image Preprocessing

For the SAM-based segmentation, no preprocessing was required. The model processed the raw images directly using automatic prompts.

For the pixel-based method, image quality and wound boundary clarity were more critical. Since real wounds often lacked clear color contrast, an interactive boundary selection tool was used to quickly mark the ROI edges. This enhanced segmentation accuracy without requiring full manual annotation.

SAM-Based Method: The Segment Anything Model (SAM) was used to automatically segment both the wound and the 1 cm^2 reference marker. The number of pixels in the reference mask established the pixel-to-cm^2 scale. This scale was applied to convert the pixel count of the segmented wound area into real-world area units. Length and width were derived from the bounding box enclosing the wound mask.

Pixel-Based Method: The grayscale or color image was processed using intensity thresholding where feasible. In cases with poor contrast, a rapid manual boundary selection was performed to isolate the wound area. The number of pixels in the wound mask was converted to cm^2 using the same scale derived from the reference marker.

4.3. Evaluation Metrics

Relative Error (%) for synthetic shapes:

$$Relative\ Error\ (\%) = \frac{|Assessed\ Area - True\ Area|}{True\ Area} * 100 \quad (15)$$

5. RESULTS

5.1. Step 1: Validation with Known Shapes, Pixel-based

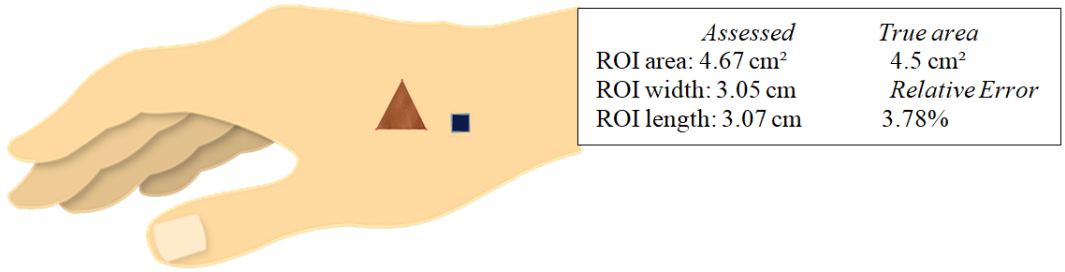

Fig. 4: Object1- ROI Estimation, Object (left) and Reference marker (right: 1 x 1 cm)

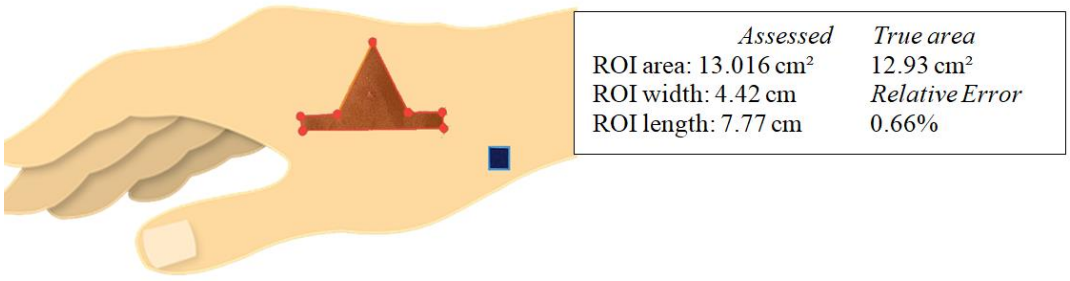

Figure 5. Object2- ROI Estimation, Object (left) and Reference marker (right: 1 x 1 cm)

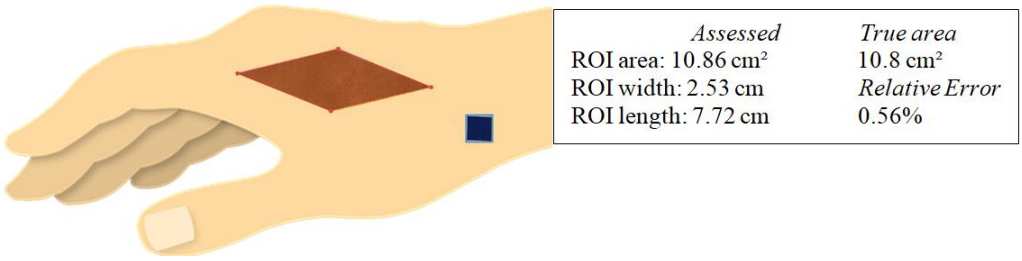

Figure 6. Object3- ROI Estimation, Object (left) and Reference marker (right: 1 x 1 cm)

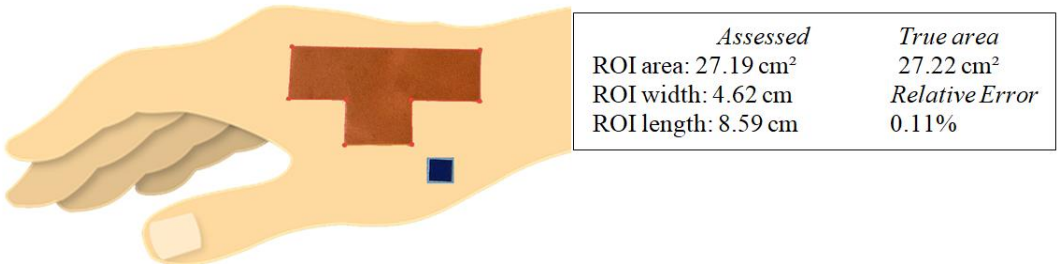

Figure 7. Object4- ROI Estimation, Object (left) and Reference marker (right: 1 x 1 cm)

5.2. Step 2: Comparison of Pixel-based and SAM Approaches for Known Shapes

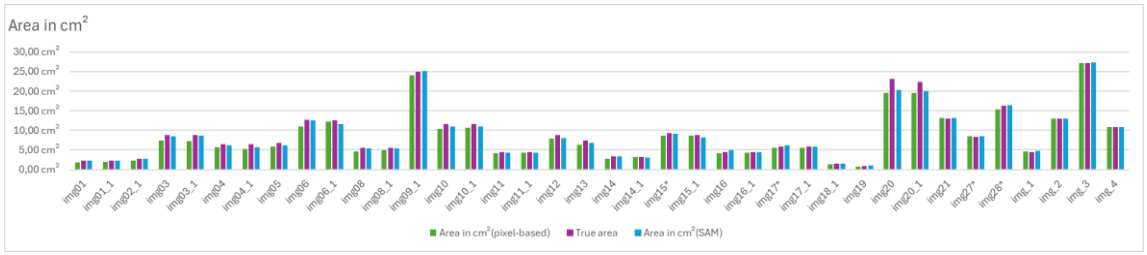

Figure 8. Assessed ROI area (pixel-based, true area and SAM) in cm²

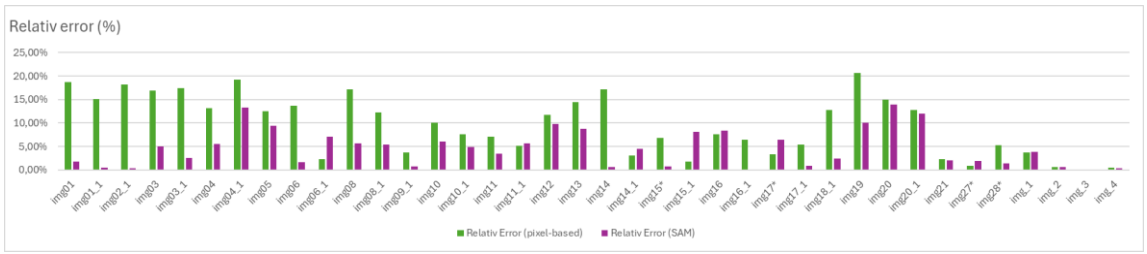

Figure 9. Relative Errors of Assessed ROI area (pixel-based vs SAM) in %

5.3. Step 3: Application on Real Wounds, Pixel-based and Deep-Learning SAM Approaches

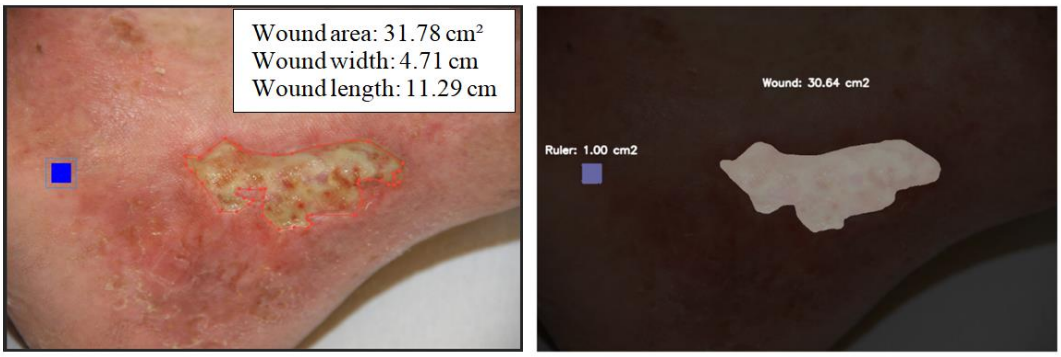

Figure 10. Wound1-Area assessment, pixel-based (left) and deep learning model SAM (right)

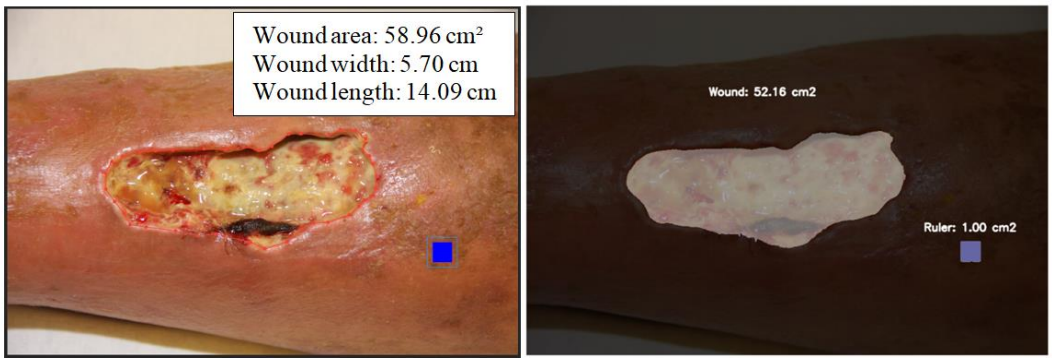

Figure 11. Wound2 -Area assessment, pixel-based (left) and deep learning model SAM (right)

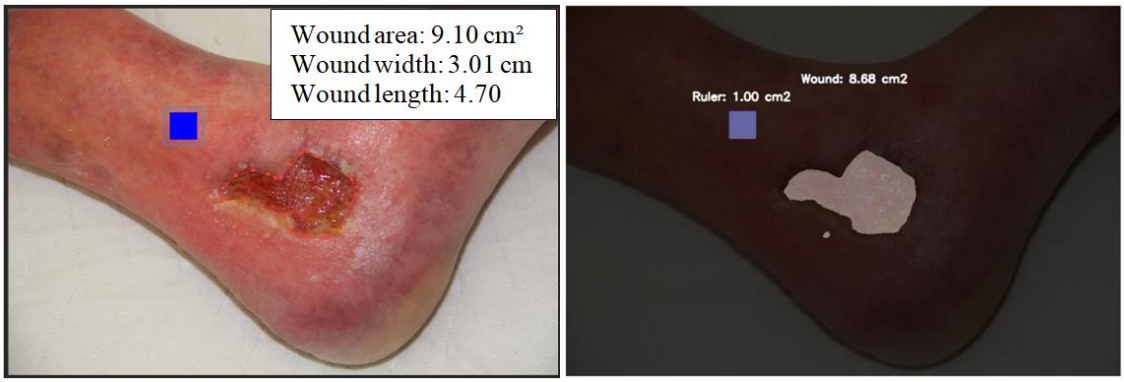

Figure 12. Wound3-Area assessment, pixel-based (left) and deep learning model SAM (right)

6. DISCUSSION

The findings of this study confirm the effectiveness of automated Region of Interest (ROI) area estimation for dermatological imaging, particularly in wound assessment. By presenting two distinct yet complementary methods: a deep learning-based approach using the Segment Anything Model (SAM) and a pixel-based thresholding method. This work addresses the need for both high-performance AI-driven solutions and lightweight, accessible alternatives suitable for resource-constrained environments.

Figures 4–7 illustrate how the experimental phases were conducted to compare the pixel-based and SAM-based approaches. In the first phase, validation was performed using geometric shapes with precisely known areas, each placed adjacent to a 1 cm² reference marker.

Results shown in Figures 8 and 9 provide a comparative evaluation of the two methods across 40 synthetic samples. The SAM-based approach consistently outperformed the pixel-based method in terms of both accuracy and robustness. Quantitatively, the average relative error for the pixel-based method was 9.5%, while the SAM-based approach achieved a significantly lower average error of 4.63%, indicating a nearly 50% reduction in estimation error. This improvement is not only statistically significant but also clinically meaningful for precise wound size tracking in treatment planning and monitoring.

Further analysis revealed that 25 out of 40 SAM-segmented cases had errors ≤5%, compared to only 11 in the pixel-based method. This highlights SAM's improved consistency, especially in challenging visual conditions such as irregular wound shapes or variable lighting. While the pixel-based method showed acceptable performance (error <4%) in simpler, well-contrasted cases, it exhibited errors exceeding 15–20% in more complex scenarios, primarily due to sensitivity to color variation, noise, and inconsistent boundary detection. In contrast, SAM maintained relatively low errors across diverse cases, benefiting from its transformer-based generalization capabilities.

In the second phase, the pixel-based method was applied to real patient images and successfully estimated wound areas in three cases. Standardized imaging conditions, such as a parallel camera angle and use of blue 1×1 cm markers, ensured accurate scaling. The method also provided useful length and width metrics essential for clinical monitoring (Figures 10–12, left).

In the third phase, the same task was repeated using the SAM-based model. Without retraining or domain-specific fine-tuning, SAM accurately segmented both the reference and wound regions,

confirming its capacity as a generalizable, high-precision tool for wound area estimation with minimal manual intervention (Figures 10–12, right).

A key strength of the proposed system is the use of consistent square reference markers, which enables reliable pixel-to-centimeter conversion. This simplicity improves adaptability and removes the need for complex calibration or proprietary tools. Although uniform markers were used, SAM's flexibility allows it to handle wounds of varying shapes and irregular contours without requiring geometry-specific references.
Importantly, the proposed framework is not limited to wound care. The same methodology can be extended to other diagnostic domains such as rheumatoid arthritis, where accurate measurement of inflamed joint regions could support disease monitoring and treatment evaluation.
Limitations and Challenges:

Despite the positive results, several limitations must be considered:

- Resolution Sensitivity: The accuracy of pixel-based estimation depends on image resolution. Lower resolution may obscure fine details, especially in small or intricate wounds. Future work could explore resolution-agnostic enhancements such as super-resolution preprocessing or multi-scale modeling.
- Challenging Wound Boundaries: For wounds with indistinct or irregular edges, the SAM model performs well, but extreme variability may still pose difficulties. Additional refinement using attention-guided masking or edge-aware segmentation could further improve accuracy.
- Reference Object Placement: Although controlled during this study, real-world placement of the reference marker could vary, affecting the scale calculation. Future work may explore automated reference detection or markerless scale estimation approaches.
- Generalizability Across Populations: While the study included both synthetic and real data, broader validation across diverse skin tones, lighting conditions, and wound types is necessary to ensure fairness and clinical reliability.

7. CONCLUSION AND FUTURE WORK

Summary of Contributions

This study introduced and evaluated two complementary methods for automated wound area estimation in dermatological images: a deep learning-based approach using the Segment Anything Model (SAM) and a classical pixel-based thresholding technique. Both methods relied on a reference marker of known dimensions (1×1 cm) to convert segmented regions from pixels to real-world area measurements (in cm^2).

Three experimental phases were conducted:

1. Phase 1 validated both methods using 40 images containing artificial shapes with known true areas. The SAM-based method achieved a significantly lower average relative error of 4.63%, compared to 9.5% for the pixel-based method. Additionally, SAM produced errors $\leq$5% in 25 out of 40 cases, versus only 11 cases for the pixel-based approach. These results confirm the higher accuracy, consistency, and robustness of the SAM approach, particularly in complex or variable imaging conditions.
2. Phase 2 applied the pixel-based method to images of real patient wounds, successfully estimating wound area, length, and width in three clinical cases. The method benefited

from consistent imaging protocols, including the use of blue 1×1 cm markers and parallel camera orientation.

3. Phase 3 tested the SAM-based method on the same clinical images. Without any task-specific retraining or fine-tuning, SAM accurately segmented both the reference and wound regions, confirming its generalization capability and clinical applicability.

Together, these contributions show that accurate, scalable wound area estimation is achievable with minimal equipment and varying levels of computational complexity. The approach has broader potential applications in other areas of medical imaging, including inflammation assessment in rheumatoid arthritis.

Future Research Directions:

Future work could involve integrating both methods into a hybrid framework that dynamically selects the optimal technique based on image quality and computational resources. Additionally, expanding this system to other medical imaging tasks, such as inflammation detection in rheumatoid arthritis or uveitis analysis in ophthalmology could validate its broader utility. Enhancing user interfaces and embedding clinical feedback mechanisms will also be critical for real-world deployment.

ACKNOWLEDGMENTS

This research was supported by the European Union, European Regional Development Fund under the program 'Promotion of Research, Development, and Innovation'. We would like to acknowledge that Authors A. Arnold and S. Lutze contributed equally in a senior supervisory role to this work.

REFERENCES

[1] P. Foltynski, A. Ciechanowska, and P. Ladyzynski, "Wound surface area measurement methods," *Biocybernetics and Biomedical Engineering*, vol. 41, no. 4, pp. 1454–1465, Oct.–Dec. 2021, doi: 10.1016/j.bbe.2021.09.009.

[2] D. K. Lee et al., "The accuracy of manual wound measurement techniques," *Wound Repair and Regeneration*, vol. 25, no. 6, pp. 789–795, 2017.

[3] H. R. Patel and J. B. Collins, "Pixel-based techniques for wound area estimation," *Journal of Digital Imaging*, vol. 31, no. 3, pp. 291–298, 2019.

[4] X. Y. Zhang et al., "Deep learning in medical image analysis: A review," *Journal of Healthcare Engineering*, vol. 2019, pp. 1–9, 2019.

[5] R. A. Williams and T. S. John, "Deep learning for wound analysis: A study of CNN-based models for wound size estimation," *Medical Image Analysis*, vol. 45, pp. 59–67, 2020.

[6] H. Carrión, M. Jafari, M. D. Bagood, H. Y. Yang, R. R. Isseroff, and M. Gomez, "Automatic wound detection and size estimation using deep learning algorithms," *PLoS Computational Biology*, vol. 18, no. 3, p. e1009852, Mar. 2022, doi: 10.1371/journal.pcbi.1009852.

[7] R. E. Carrión et al., "Automatic wound detection and size estimation using deep learning for monitoring wound healing," *PLOS ONE*, vol. 17, no. 3, p. e0264574, 2022, doi: 10.1371/journal.pone.0264574.

[8] R. Chairat et al., "Detect-and-segment: A deep learning approach to automate wound detection and segmentation," *Computers in Biology and Medicine*, vol. 145, p. 105429, 2022, doi: 10.1016/j.compbiomed.2022.105429.

[9] C. W. Chang et al., "Deep learning approach based on superpixel segmentation assisted labeling for automatic pressure ulcer diagnosis," *PLOS ONE*, vol. 17, no. 2, p. e0264139, 2022, doi: 10.1371/journal.pone.0264139.

[10] P. Foltynski and P. Ladyzynski, "Evaluation of two digital wound area measurement methods using artificial intelligence," *Electronics*, vol. 13, no. 12, p. 2390, 2022, doi: 10.3390/electronics13122390.

[11] D. Y. T. Chino et al., "Segmenting skin ulcers and measuring the wound area using deep convolutional networks," *Computer Methods and Programs in Biomedicine*, vol. 191, Jul. 2020, doi: 10.1016/j.cmpb.2020.105376.

[12] C. Liu, X. Fan, Z. Guo, et al., "Wound area measurement with 3D transformation and smartphone images," *BMC Bioinformatics*, vol. 20, p. 724, 2019, doi: 10.1186/s12859-019-3308-1.

[13] F. Ferreira et al., "Experimental study on wound area measurement with mobile devices," *Sensors*, vol. 21, no. 17, p. 5762, 2021, doi: 10.3390/s21175762.

[14] T. J. Liu, H. Wang, M. Christian, and C.-W. Chang, "Automatic segmentation and measurement of pressure injuries using deep learning models and a LiDAR camera," *Scientific Reports*, vol. 13, no. 1, Jan. 2023, doi: 10.1038/s41598-022-26812-9.

[15] M. C. Alonso, H. T. Mohammed, R. D. J. Fraser, and J. L. Ramírez-GarcíaLuna, "Comparison of wound surface area measurements obtained using clinically validated artificial intelligence-based technology versus manual methods and the effect of measurement method on debridement code reimbursement cost," *Wounds: A Compendium of Clinical Research and Practice*, vol. 35, no. 10, pp. E331–E338, Oct. 2023, doi: 10.25270/wnds/2303.

[16] K. Löwenstein et al., "Virtually objective quantification of in vitro wound healing scratch assays with the Segment Anything Model," *arXiv preprint*, arXiv:2407.02187, 2024. [Online]. Available: https://arxiv.org/abs/2407.02187

[17] Labellerr, "Enhancing wound image segmentation with Labellerr," Labellerr Blog, 2023. [Online]. Available: https://www.labellerr.com/blog/enhancing-wound-image-segmentation/

[18] I. Morales-Ivorra, J. Narváez, C. Gómez-Vaquero, C. Moragues, J. M. Nolla, J. A. Narváez, and M. A. Marín-López, "Assessment of inflammation in patients with rheumatoid arthritis using thermography and machine learning: a fast and automated technique," *RMD Open*, vol. 8, no. 2, p. e002458, Jul. 2022, doi: 10.1136/rmdopen-2022-002458.

[19] U. Snekhalatha, M. Anburajan, V. Sowmiya, B. Venkatraman, and M. Menaka, "Automated hand thermal image segmentation and feature extraction in the evaluation of rheumatoid arthritis," Proceedings of the Institution of Mechanical Engineers, Part H: *Journal of Engineering in Medicine*, vol. 229, no. 4, pp. 319–331, Apr. 2015, doi: 10.1177/0954411915580809.

[20] A. N. Wilson, K. A. Gupta, B. H. Koduru, A. Kumar, A. Jha, and L. R. Cenkeramaddi, "Recent advances in thermal imaging and its applications using machine learning: A review," *IEEE Sensors Journal*, vol. 23, no. 4, pp. 3395–3407, Feb. 2023, doi: 10.1109/JSEN.2023.3234335.

[21] A. Alshehri and D. AlSaeed, "Breast cancer detection in thermography using convolutional neural networks (CNNs) with deep attention mechanisms," *Applied Sciences*, vol. 12, no. 24, p. 12922, 2022, doi: 10.3390/app122412922.

[22] S. J. Mambou, P. Maresova, O. Krejcar, A. Selamat, and K. Kuca, "Breast cancer detection using infrared thermal imaging and a deep learning model," *Sensors*, vol. 18, no. 9, p. 2799, Aug. 2018, doi: 10.3390/s18092799.

[23] Y. Qu, Y. Meng, H. Fan, and R. X. Xu, "Low-cost thermal imaging with machine learning for non-invasive diagnosis and therapeutic monitoring of pneumonia," *Infrared Physics & Technology*, vol. 123, p. 104201, Jun. 2022, doi: 10.1016/j.infrared.2022.104201.

[24] R. Gulias-Cañizo, M. E. Rodríguez-Malagón, L. Botello-González, V. Belden-Reyes, F. Amparo, and M. Garza-Leon, "Applications of infrared thermography in ophthalmology," *Life*, vol. 13, no. 3, p. 723, 2023, doi: 10.3390/life13030723.

[25] J. Wang, Y. Tian, T. Zhou, D. Tong, J. Ma, and J. Li, "A survey of artificial intelligence in rheumatoid arthritis," *Rheumatology and Immunology Research*, vol. 4, no. 2, pp. 69–77, Jul. 2023, doi: 10.2478/rir-2023-0011.

[26] I. Morales-Ivorra, D. Taverner, O. Codina, S. Castell, P. Fischer, D. Onken, P. Martínez-Osuna, C. Battioui, and M. A. Marín-López, "External validation of the machine learning-based thermographic indices for rheumatoid arthritis: A prospective longitudinal study," *Diagnostics*, vol. 14, no. 13, p. 1394, Jun. 2024, doi: 10.3390/diagnostics14131394.

[27] V. Shenoy et al., "Deepwound: Automated postoperative wound assessment and surgical site surveillance through convolutional neural networks," *arXiv preprint*, arXiv:1807.04355, 2018. [Online]. Available: https://arxiv.org/abs/1807.04355

[28] D. M. Anisuzzaman et al., "A mobile app for wound localization using deep learning," *arXiv preprint*, arXiv:2009.07133, 2020. [Online]. Available: https://arxiv.org/abs/2009.07133

[29] C. W. Chang et al., "A superpixel-driven deep learning approach for the analysis of dermatological wounds," *Computer Methods and Programs in Biomedicine*, vol. 178, p. 105079, 2019, doi: 10.1016/j.cmpb.2019.105079.

[30] H. Nejati et al., "Fine-grained wound tissue analysis using deep neural network," *arXiv preprint*, arXiv:1802.10426, 2018. [Online]. Available: https://arxiv.org/abs/1802.10426

[31] I. Ballester, M. Gall, T. Münzer, et al., "Depth-based interactive assistive system for dementia care," *Journal of Ambient Intelligence and Humanized Computing*, vol. 15, pp. 3901–3912, 2024, doi: 10.1007/s12652-024-04865-0.

AUTHORS

Rolf-Dietrich Berndt is a German engineer and Managing Director of Infokom GmbH, an ICT company in Neubrandenburg, Germany. He specializes in eHealth innovation, focusing on telemedicine, mobile health (mHealth), and digital chronic care solutions. He is a certified expert in data security and privacy and holds ISO 27001 ISMS certification. Berndt has led the development of secure, interoperable platforms such as mSkin® for teledermatology and Mobil Diab® for diabetes management, applied in both European and African healthcare contexts. His work emphasizes accessible, privacy-compliant technologies linking primary care, specialists, and hospitals

Claude Takenga holds a BSc and MSc in Radio Engineering and Telecommunication, and a PhD in Electrical Engineering from Hannover University. He works in the Research and Development department at Infokom, focusing on innovation in digital health technologies. His research spans AI-based medical imaging, mobile health solutions, and eHealth systems for chronic disease management. He has led international health projects across Europe and sub-Saharan Africa, promoting scalable, digital diagnostics and telemedicine tools for underserved regions.

Petra Preik holds a Diploma in Informatics Engineering from the Fachhochschule Neubrandenburg. She works in software development at Infokom, focusing on digital health applications. Her expertise includes the design and implementation of secure, interoperable healthcare software systems and telemedicine solutions. With practical experience in clinical IT environments, she contributes to the development of user-friendly tools that support healthcare professionals and enhance patient care.

Tripura Siripurapu works in the Research and Development department at Infokom, with a primary focus on Artificial Intelligence and Deep Learning for medical imaging. Her work involves developing advanced machine learning algorithms for image segmentation, feature extraction, and diagnostic support in digital health applications. She contributes to projects aimed at enhancing the accuracy and efficiency of clinical image analysis.

Thomas A. Fuchsluger (Univ.-Prof. Dr. med. Dr. rer. nat) is a renowned specialist - scientist with dual doctorates in medicine and natural sciences. He serves as the Chair of Ophthalmology at the University of Rostock. His clinical and research expertise includes corneal transplantation, ocular surface diseases, and regenerative therapies. Prof. Fuchsluger has published extensively in peer-reviewed journals and leads multiple interdisciplinary projects at the intersection of ophthalmology, tissue engineering, and digital health. His work contributes significantly to advancing personalized eye care and clinical innovation in ophthalmic surgery.

Christoph Lutter (Univ.-Prof. Dr. med.) is a specialist in orthopedic surgery and traumatology, with a strong focus on musculoskeletal research and clinical innovation. He holds a professorship at the University of Rostock and leads initiatives in orthopedic regenerative medicine, joint preservation, and advanced imaging techniques. Prof. Lutter is actively involved in translational research, integrating clinical practice with technological advancements, including AI-driven diagnostics. His work emphasizes patient-centered care and contributes to improving surgical outcomes and rehabilitation strategies in orthopedic medicine.

Andreas Arnold (Dr. med.) is a senior physician at the Clinic and Polyclinic for Skin Diseases at the University Medicine Greifswald. His areas of expertise include dermatologic oncology, digital dermatology, and clinical telemedicine. Dr. Arnold is engaged in research and development of innovative diagnostic approaches in skin cancer care, with a strong focus on integrating teleconsultation and imaging technologies into routine dermatological practice. He contributes to teaching and clinical research, supporting the advancement of patient-centered, technology-supported dermatology.

Stine Lutze (Dr. med.) is Executive Senior Physician at the Clinic and Polyclinic for Skin Diseases at the University Medicine Greifswald. Her clinical and research focus lies in skin tumors, teledermatology, and teleconsultation services. She plays a key role in advancing digital dermatological care, supporting interdisciplinary collaboration and remote diagnostics. Dr. Lutze is actively involved in both clinical practice and research contributing to innovation in patient-centered eHealth solutions.